Article

Aerosol Optical Depth over the Arctic Snow-Covered Regions Derived from Dual-Viewing Satellite Observations

Zheng Shi [1,2,†], Tingyan Xing [3,*,†], Jie Guang [1], Yong Xue [4,5,*] and Yahui Che [1,2]

[1] The Key Laboratory of Digital Earth Science, Institute of Remote Sensing and Digital Earth, Chinese Academy of Sciences, Beijing 100094, China; shizheng@radi.ac.cn (Z.S.); guangjie@aircas.ac.cn (J.G.); cheyh@radi.ac.cn (Y.C.)

[2] University of Chinese Academy of Sciences, Beijing 100049, China

[3] School of Information Engineering, China University of Geosciences (Beijing), 29 Xue Yuan Road, Haidian District, Beijing 100083, China

[4] Department of Computing and Mathematics, College of Engineering and Technology, University of Derby, Kedleston Road, Derby DE22 1GB, UK

[5] School of Environmental Science and Spatial Informatics, China University of Mining and Technology, No.1 Daxue road, Xuzhou 221116, China

[*] Correspondence: xtygis@cugb.edu.cn (T.X.); y.xue@derby.ac.uk (Y.X.)

[†] These authors contributed equally to this work.

check for updates

Abstract: Aerosol properties over the Arctic snow-covered regions are sparsely provided by temporal and spatially limited in situ measurements or active Lidar observations. This introduces large uncertainties for the understanding of aerosol effects on Arctic climate change. In this paper, aerosol optical depth (AOD) is derived using the advanced along-track scanning radiometer (AATSR) instrument. The basic idea is to utilize the dual-viewing observation capability of AATSR to reduce the impacts of AOD uncertainties introduced by the absolute wavelength-dependent error on surface reflectance estimation. AOD is derived assuming that the satellite observed surface reflectance ratio can be well characterized by a snow bidirectional reflectance distribution function (BRDF) model with a certain correction direct from satellite top of the atmosphere (TOA) observation. The aerosol types include an Arctic haze aerosol obtained from campaign measurement and Arctic background aerosol (maritime aerosol) types. The proper aerosol type is selected during the iteration step based on the minimization residual. The algorithm has been used over Spitsbergen for the spring period (April–May) and the AOD spatial distribution indicates that the retrieval AOD can capture the Arctic haze event. The comparison with AERONET observations shows promising results, with a correlation coefficient R = 0.70. The time series analysis shows no systematical biases between AATSR retrieved AOD and AERONET observed ones.

Keywords: Arctic; AATSR; AOD; snow

1. Introduction

Aerosols exert a variety of effects on both the climate and the environment, directly through scattering (e.g., cooling of the atmosphere–surface system and absorption of incoming solar radiation that cools the surface but warms the atmosphere), and indirectly through their effects on cloud formation and the microphysical properties of clouds, which in turn influences cloud albedo and precipitation [1,2]. The Arctic environment is a significant indicator of global climate change. Satellite observations and Lidar measurements have revealed the occurrence of substantial amounts of smoke

and other particulate matter in the tropopause region and lower stratosphere at high latitudes in the Arctic region [3] due to transport of anthropogenic [4] or natural aerosol particles produced by sources such as wildfires [5] and volcanic eruptions [6]. Aerosol optical depth (AOD) retrieval over the Arctic region from satellite is an important but challenging task.

Existing aerosol retrieval algorithms for passive remote sensing focus mainly on those snow/ice and cloud free regions. An overview of aerosol remote sensing in Polar regions can be found in Tomasi et al. [7]. Some instruments, especially a multi-angle imaging spectro-radiometer (MIRS), show potential capabilities for aerosol retrieval over snow and ice and has been investigated [8]. Some more recent investigations can be found in Istomina et al. [9] and Mei et al. [10,11]. Istomina et al. tried to use a dual-view method with visible wavelengths [9] and infrared [12] spectral regions to retrieve AOD over the Arctic regions using advanced along-track scanning radiometer (AATSR) data. Mei et al. have used a similar idea to retrieve AOD over the Arctic regions using both AATSR [10] and MODIS [11]. However, the above algorithms utilize a simple pure snow model [13] and one "Arctic haze" aerosol type, which may introduce retrieval biases due to the snow cover and aerosol types. This paper is a further development based on the work of Mei et al. [14]. In this paper, the pure snow bidirectional reflectance distribution function (BRDF) model has been corrected by the snow fraction estimation from the normalized-difference snow index (NDSI). A dynamic aerosol type of Arctic haze or background aerosol type is iteratively selected during the retrieval.

This paper aims to provide an attempt to derive AOD over the Arctic regions. The paper is organized in the following structure. The satellite and ground-based dataset are introduced in Section 2, the aerosol retrieval algorithms are described in Section 3, and the validation results and analysis are included in Section 4.

2. Materials

2.1. AATSR Instrument

AATSR on board the European Space Agency (ESA) ENVISAT satellite, with a lifetime of May 2002–April 2012, is the successor of ATSR-1 and ATSR-2 on board ERS-1 (launched in 1991) and ERS-2 (launched in 1995). AATSR data provide observations with a resolution of 1 km at nadir and a swath of 512 km. AATSR has the dual-viewing observation capability (with a forward view angle of 55°) for several wavelengths from visible to thermal infrared channels (0.55, 0.66, 0.87, 1.6, 3.7, 11 and 12 μm). AATSR series are initially designed to provide the sea surface temperature (SST) product with an accuracy of 0.3K required for climate research. However, it now also plays important roles in many application areas such as vegetation, aerosol, and cloud. The successor of AATSR is the Sea and Land Surface Temperature Radiometer (SLSTR) onboard Sentinel-3A and Sentinel-3B, which were launched on February 2016 and April 2018, respectively. Sentinel-3A is part of the European Global Monitoring for Environment and Security (GMES) program. ATSR-1/ATSR-2/AATSR/SLSTR will create a long-term data record for climate change research.

2.2. AERONET

The Aerosol Robotic Network (AERONET) is a globally distributed network of over 800 stations which provides high quality aerosol optical properties that are widely used for various aerosol-related studies, such as the validation of satellite retrieved AOD products [15,16]. AERONET uses the CIMEL sun/sky radiometers to obtain direct sun and diffuse sky radiances within the 340–1020 nm and 440–1020 nm spectral ranges, respectively. AOD measurements are recorded every 15 min from direct solar radiation, with an accuracy of 0.01–0.02 at visible wavelengths [15]. AERONET data can be downloaded from the official website (http://aeronet.gsfc.nasa.gov/). The AOD values at 550 nm are not directly provided by AERONET, and are interpolated from AERONET AODs at 440 nm and 870 nm using the Ångström equation, the accuracy of which is proven to be sufficient [17].

3. Methods

The main idea of this retrieval algorithm is to use the dual-viewing observation capability of the AATSR instrument. The algorithm has been described in Mei et al. [14]. Here, we give a summary of the algorithm. The algorithm assumes that the surface reflectance can be approximated by two parts: One describes the variation with the wavelength and the other is to describe the variation with the geometry [18]. The surface reflectance ratio is mainly affected by the surface BRDF shape and can reduce the impact from the absolute value of surface directional reflectance [19]. This idea can be used to mitigate the requirement of a precise pre-calculation of wavelength-dependent surface reflectance, which is helpful for very bright surface such as snow/ice covered regions [9,12]. This can be illustrated as the following equation:

$$\frac{\rho^f_{sfc}(\lambda,\mu_0,\mu,\phi)}{\rho^n_{sfc}(\lambda,\mu_0,\mu,\phi)} = \frac{\rho^f_{TOA}(\lambda,\mu_0,\mu,\phi) - \rho^f_{atm}(\lambda,\mu_0,\mu,\phi)}{\rho^n_{TOA}(\lambda,\mu_0,\mu,\phi) - \rho^n_{atm}(\lambda,\mu_0,\mu,\phi)} \times \frac{T^n(\lambda,\mu)}{T^f(\lambda,\mu)} \tag{1}$$

where $\rho_{sfc}(\lambda,\mu_0,\mu,\phi)$ is the surface reflectance, $\rho_{TOA}(\lambda,\mu_0,\mu,\phi)$ is the satellite observed TOA reflectance, $\rho_{atm}(\lambda,\mu_0,\mu,\phi)$ is the atmospheric reflectance, $T(\lambda,\mu)$ is the total (upward and downward directions) atmospheric transmittance, and f and n indicate AATSR forward and nadir observation angles, respectively.

We can re-write Equation (1) as

$$\frac{\rho^f_{sfc}(\lambda,\mu_0,\mu,\phi)}{\rho^n_{sfc}(\lambda,\mu_0,\mu,\phi)} = \frac{\Delta\rho^f(\lambda,\mu_0,\mu,\phi)}{\Delta\rho^n(\lambda,\mu_0,\mu,\phi)} \times \frac{\Delta\rho^n(\lambda,\mu_0,\mu,\phi) \times s + T^n(\lambda,\mu)}{\Delta\rho^f(\lambda,\mu_0,\mu,\phi) \times s + T^f(\lambda,\mu)} \tag{2}$$

$$\Delta\rho(\lambda,\mu_0,\mu,\phi) = \rho_{TOA}(\lambda,\mu_0,\mu,\phi) - \rho_{atm}(\lambda,\mu_0,\mu,\phi) \tag{3}$$

where s is the hemispheric atmospheric reflectance, which depends on the aerosol loading and type.

The key issue for Equation (2) is to decouple the contribution of aerosol from surface signal. Therefore, a proper snow BRDF model, depending on the viewing and illumination angle, wavelength, and snow properties such as size and shape of grains [20–22], which can characterize both AATSR observation directions, is needed. A snow BRDF model was selected as following [21]:

$$R(\mu,\mu_0,\phi) = R_0(\mu,\mu_0,\phi)A^{f(\mu,\mu_0,\phi)} \tag{4}$$

where

$$A = \exp\{\frac{-4s}{\sqrt{3}}\}, \; s = \sqrt{\frac{1-\varpi}{1-g\varpi}},$$

$$f = \frac{u(\mu)u(\mu_0)}{R_0(\mu,\mu_0,\phi)}, u(\mu) = \frac{3}{7}(1+2\mu)$$

$$R_0(\mu,\mu_0,\phi) = \frac{a + b(\mu+\mu_0) + c\mu\mu_0 + p(\phi)}{4(\mu+\mu_0)}$$

where $R_0(\mu,\mu_0,\phi)$ is the reflection function for non-absorbing snow layer, g is the asymmetry factor of snow particle, ϖ is the single scattering albedo, $a = 1.247$, $b = 1.186$, $c = 5.157$, ϕ is the scattering angle, $p(\theta) = 11.1\exp(-0.087\theta) + 1.1\exp(-0.014\theta)$, $\mu_0 = \cos\theta_0$, θ_0 and θ are solar zenith angle and satellite zenith angle, respectively.

Only pure snow-covered area is used for the retrieval and in the real AATSR measurements some corrections are needed in order to take the snow structure into account. Istomina (2009) used the following equation [9]:

$$\frac{\rho_{sfc}^{f}(\lambda,\mu_0,\mu,\phi)}{\rho_{sfc}^{n}(\lambda,\mu_0,\mu,\phi)} = \frac{\rho_{sfc,sim}^{f}(\lambda,\mu_0,\mu,\phi)}{\rho_{sfc,sim}^{n}(\lambda,\mu_0,\mu,\phi)} \frac{\rho_{TOA,sim}^{n}(\lambda,\mu_0,\mu,\phi)}{\rho_{TOA,sim}^{f}(\lambda,\mu_0,\mu,\phi)} \frac{\rho_{TOA}^{f}(\lambda,\mu_0,\mu,\phi)}{\rho_{TOA}^{n}(\lambda,\mu_0,\mu,\phi)} \tag{5}$$

Equation (5) tries to mitigate the atmospheric effect of $\rho_{TOA}(\lambda,\mu_0,\mu,\phi)$ by modelled $\rho_{sfc,sim}(\lambda,\mu_0,\mu,\phi)$ and $\rho_{TOA,sim}(\lambda,\mu_0,\mu,\phi)$ ratio.

Mei et al. [14] proposed another way to take this effect into account. The main idea is that the "real snow" BRDF can be better estimated from the original BRDF model [21] with a correction term by the snow cover fraction (SCF). The SCF can be calculated by an empiric relationship from NDSI. The NDSI is defined as following:

$$\text{NDSI} = \frac{\rho_{0.55} - \rho_{1.6}}{\rho_{0.55} + \rho_{1.6}} \tag{6}$$

The SCF was then estimated using the following empirical equation [23]:

$$\text{SCF} = 1.21 \times \text{NDSI} + 0.06 \tag{7}$$

Then, the snow BRDF ratio can be rewritten as following:

$$\frac{\rho_{sfc}^{f}(\lambda,\mu_0,\mu,\phi)}{\rho_{sfc}^{n}(\lambda,\mu_0,\mu,\phi)} = \frac{\rho_{sfc,sim}^{f}(\lambda,\mu_0,\mu,\phi) \times \text{SCF}^{f}}{\rho_{sfc,sim}^{n}(\lambda,\mu_0,\mu,\phi) \times \text{SCF}^{n}} \tag{8}$$

One important aerosol property is the aerosol phase function. In this paper two aerosol types were used: One is a background aerosol type and the other is an Arctic haze type. The phase functions for those two types are presented in Figure 1. The Arctic haze aerosol is measured during the Arctic haze event on 23 March 2003 at Spitsbergen (78.923N, 11.923E). Following this, the look-up-table was calculated using 6S radiative transfer package [19].
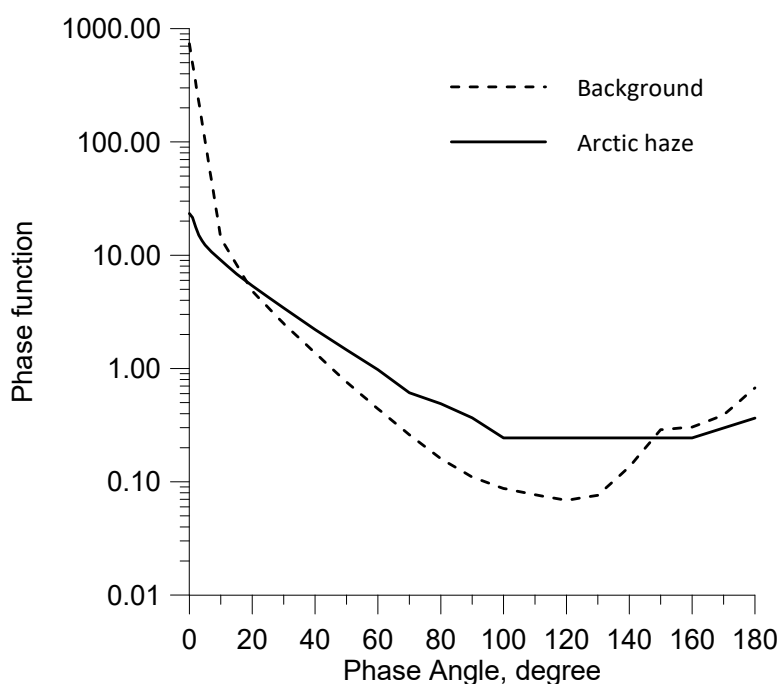

Figure 1. Phase function of two aerosol types used in the retrieval (adapted from [9]).

4. Results and Discussions

Aerosol retrieval over the snow/ice covered Arctic regions is new and difficult. The retrieved results must be evaluated by comparing them with in situ measurements, such as those from AERONET and other satellite products. However, there are limited in situ observations. Thus, we used a two-step validation strategy to overcome this problem. The first step was to check if the retrieved results can qualitatively characterize the famous Arctic haze event by checking a series of retrieval days and to investigate the AOD before, during and after the Arctic haze event. It is reported that a serious Arctic haze event happened in April and May 2006, due to a large number of agriculture biomass burning (fires burned in the forests of the nature preserve at Kuronian Spit, Lithuania) that occurred in the Baltic countries, western Russia, Belarus, and the Ukraine, which were monitored by Stohl et al. [24]. The air mass brought pollutants from mid-latitudes to Arctic regions such as Spitsbergen during this period. The most severe air pollution episodes happened on 27 April and during early May 2006, when the concentrations of most measured air pollutants (aerosols, O3, etc.) exceeded previously recorded long-term maxima [24].

Figure 2 shows the AOD time series over Spitsbergen for the above-mentioned Arctic haze event. Due to high cloud coverage, Spitsbergen is mostly covered by cloud; thus, Figure 2 picks up those days in the haze event with relatively lower cloud cover. According to Figure 2, the retrievals show smooth patterns that do not match the surface structures according to visual checking using the RGB images, indicating the decoupling of surface and aerosol in the retrieval algorithm. Figure 2 shows the before, during, and after Arctic haze period. The dates 29 March and 1 April were before the haze period and we can see that the AOD at 550 nm values are extremely low with values of less than 0.1 or even lower than 0.05, indicating the clean air condition of Arctic due to a lack of local emissions. The main aerosol source in the Arctic without transport from middle–low latitudes is mainly sea spray aerosol from the surrounding ocean [25], and the properties of the so-called Arctic aerosol type can be found in optical properties of aerosols and clouds (OPAC) [26], with an aerosol loading of less than 0.05. As presented in [24], the severe haze event started in early May. We show the period of 2–4 May 2006. We can see some high AODs (AOD > 0.5) with a certain cloud pattern, which was probably due to cloud contamination. The cloud screening algorithm developed by Istomina et al. [27] has been proving to have remaining clouds. Due to the cloud screening over this region, an image processing procedure, such as post-processing, will be helpful to further improve the retrieval quality [28]. We can see that the Arctic haze started in early April 2006. High AOD (AOD > 0.15) can be observed at southern Spitsbergen, indicating aerosol transport from middle latitude. The haze event reaches its peak on 2–4 May, which is in accordance with the smoke transported from Eastern Europe in agricultural fire events [24]. The AOD values were larger than 0.2 and some reached 0.3. The haze event started to decrease in mid-May. Beside the problem of potential cloud contamination, another problem is linked to the surface BRDF properties. We have checked the RGB figures for some corresponding days and some surface structure may also contribute to the high "hot spots" in the retrieval. The snow/ice BRDF model used in the retrieval is proposed based on assumptions which may lack parameters to describe the surface textures [10]; thus, a new surface BRDF model based on campaign measurement is under development. The above results show that the satellite retrieved AOD can qualitatively describe the Arctic haze event reasonably well. It is novel to see the Arctic haze event in a time series, rather than on only one day as presented in Mei et al. [14], from passive remote sensing.

The second step of the evaluation was to quantitatively compare retrieved AOD results with AERONET observations. The longest observation site over Hornsund (77.001°N, 15.540°E) was used. Figure 3 shows the comparison between satellite retrieval and AERONET for the Arctic haze period during 2006–2009. Relatively good agreement is found between satellite retrieval and AERONET observations, with a correlation coefficient of R = 0.70 and regression equation of y = (0.83 ± 0.12)x + (0.02 ± 0.01). However, a relatively large RMSE of 0.03 (Arctic normal condition) can be seen in the limited validation. A better slope compared to Mei et al. [10], which has been clarified due to the BRDF ratio estimation error and the gas effect on long wavelength such as 870 nm,

shows that the improvement of the retrieval was due to a better surface parametrization and aerosol type assumption. In Mei et al. [10,11,14], only an Arctic haze aerosol is used for all cases, while in this study the aerosol type was selected during the iteration steps by checking the AOD value of each step.

In order to have a clear view of each retrieval point, a time series of satellite retrieved and AERONET observed AODs are presented in Figure 4. According to Figure 4, satellite retrieval detected similar patterns to AERONET, indicating the good performance of satellite retrieved AOD for describing Arctic haze events, as presented before. However, satellite retrieval tends to underestimate the low-AODs and overestimate high-AODs, indicating that the potential aerosol optical (particle size distribution and reflective indices) properties may need to be further adjusted. This haze event has also been described in Mei et al. [11] using a Moderate Resolution Imaging Spectroradiometer (MODIS) retrieval, and the magnitude of AOD for 29 March 2006 is about 0.07–0.09, while it is about 0.2 for 3 May 2006, which agrees well with this retrieval.
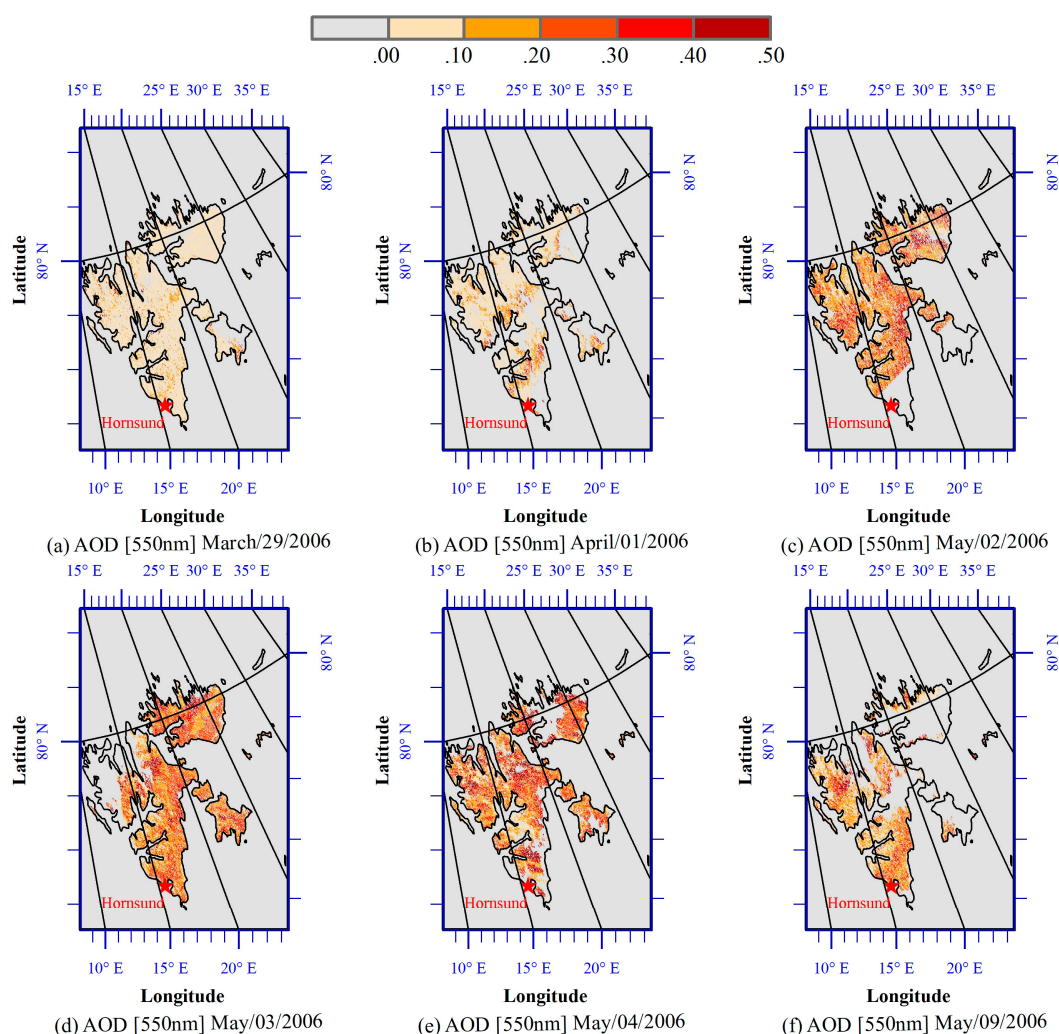
Figure 2. Advanced along-track scanning radiometer (AATSR) derived aerosol optical depth (AOD) at 550 nm for a haze event reported in Stohl et al. (2007) for selected days before, during and after the haze event: (**a**) 29 March, (**b**) 1 April, (**c**) 2 May, (**d**) 3 May, (**e**) 4 May, and (**f**) 9 May.
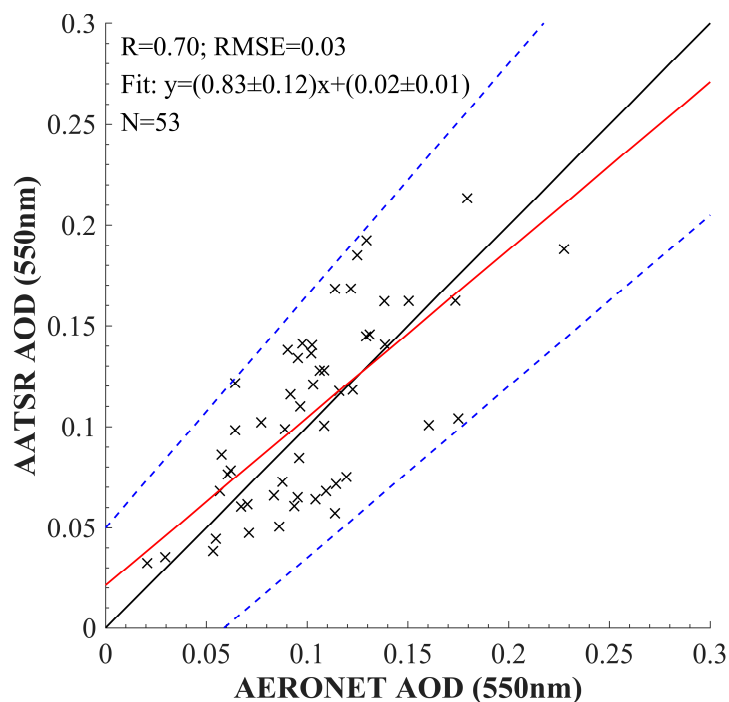
Figure 3. Validation of AATSR derived AOD at 550 nm compared to AERONET AOD.
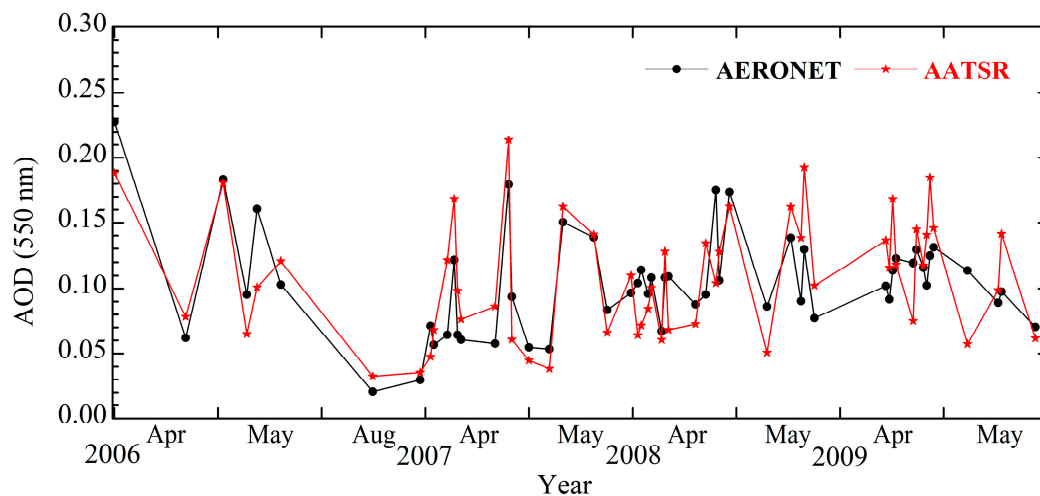

Figure 4. Time series of AATSR derived AOD at 550 nm compared to AERONET AOD.

5. Conclusions

An attempt for the retrieval of AOD over the Arctic regions based on the work in Mei et al. [10,11,14] has been proposed in this paper using an AATSR instrument. The algorithm uses the ratio of the dual-viewing observation of AATSR to minimize the requirements from highly-accurate, wavelength-dependent, absolute surface reflectance. The ratio of two views can be well characterized by a snow BRDF model with some corrections. Two aerosol types (background aerosol and Arctic haze aerosol) have been selected during the iterative process. The retrieval is based on the LUT method.

This paper presents the retrieved AOD for April and May between 2006–2009 over Spitsbergen. A haze event was well-captured by the AATSR derived AOD. The Arctic haze due to the transport of biomass burning plume from mid-latitudes reached Spitsbergen in early April and the impacts decreased during the middle of May, which agreed with the AERONET observation. The validation against AERONET shows promising retrievals, with a correlation coefficient of R = 0.70 and all

match-up points falling into ±0.05 ± 15%τ. It should be noted that only the pure snow-covered (with minor surface structures, such as texture and shadow) non-cloud-contaminated scenarios were manually selected and confirmed in the validation. The retrievals with potential effects from cloud contamination or surface structures are labeled as low-quality, and were not included in the validation. However, an RMSE of 0.03 was observed, which is high for the Arctic region. The time series compared to AERONET shows that AATSR-derived AOD in general tends to overestimate AOD, which may due to the surface parameterization and uncertainties of aerosol types in the Arctic regions. However, AATSR-derived AOD catches most of the Arctic haze peaks.

Although some promising results have been achieved, there are still problems which need to be further addressed in future work. The first problem comes from the cloud screening or pure snow pixel selection, as the current cloud screening/snow pixel selection may introduce some cloud contamination; resultantly, there are high AOD biases in the retrieval. A more robust cloud screening utilizing time series may be introduced in the future [29]. The second problem is the correction term introduced here ignoring other surface contributions, which may underestimate the surface reflectance ratio, and thus overestimate AOD. This part may be improved by a full radiative calculation using existing snow BRDF measurements such as those in Clémence et al. [30]. The overestimation of low-AODs and underestimation of high-AODs may also be attributed to the aerosol types. The optical properties of the two selected aerosol types, mainly the particle size distribution and aerosol absorption, may need some updates based on more observations. A more suitable aerosol type is still needed based on more campaign measurements.

Author Contributions: Data curation, Z.S. and T.X.; Formal analysis, Z.S., T.X., J.G. and Y.C.; Funding acquisition, J.G.; Methodology, Z.S. and T.X.; Supervision, Y.X.; Validation, Z.S. and Y.C.; Visualization, Y.C.; Writing—Original Draft Preparation, Z.S.; Writing—Review & Editing, T.X., J.G. and Y.X.

Conflicts of Interest: The authors declare no conflict of interest.

References

1. Tanré, D.; Bréon, F.M.; Deuzé, J.L.; Dubovik, O.; Ducos, F.; François, P.; Goloub, P.; Herman, M.; Lifermann, A.; Waquet, F. Remote sensing of aerosols by using polarized, directional and spectral measurements within the A-Train: The PARASOL mission. *Atmos. Meas. Tech. Discuss.* **2011**, *4*, 2037–2069. [CrossRef]
2. Andreae, M.O.; Rosenfeld, D. Aerosol–cloud–precipitation interactions. Part 1. The nature and sources of cloud-active aerosols. *Earth-Sci. Rev.* **2008**, *89*, 13–41. [CrossRef]
3. Damoah, R.; Spichtinger, N.; Forster, C.; James, P.; Mattis, I.; Wandinger, U.; Beirle, S.; Wagner, T.; Stohl, A. Around the world in 17 days-hemispheric-scale transport of forest fire smoke from Russia in May 2003. *Atmos. Chem. Phys.* **2004**, *4*, 1311–1321. [CrossRef]
4. Shaw, G.E. The Arctic Haze Phenomenon. *Bull. Am. Meteorol. Soc.* **1995**, *76*, 2403–2414. [CrossRef]
5. Kim, Y.; Hatsushika, H.; Muskett, R.R.; Yamazaki, K. Possible effect of boreal wildfire soot on Arctic sea ice and Alaska glaciers. *Atmos. Environ.* **2005**, *39*, 3513–3520. [CrossRef]
6. Herber, A.; Thomason, L.W.; Dethloff, K.; Viterbo, P.; Radionov, V.F.; Leiterer, U. Volcanic perturbation of the atmosphere in both polar regions: 1991–1994. *J. Geophys. Res. Atmos.* **1996**, *101*, 3921–3928. [CrossRef]
7. Tomasi, C.; Kokhanovsky, A.A.; Lupi, A.; Ritter, C.; Smirnov, A.; O'Neill, N.T.; Stone, R.S.; Holben, B.N.; Nyeki, S.; Wehrli, C.; et al. Aerosol remote sensing in polar regions. *Earth-Sci. Rev.* **2015**, *140*, 108–157. [CrossRef]

8.   Kahn, R.; The MISR Team. Arctic Research of the Composition of the Troposphere from Aircr-aft and Satellites Home Page. Available online: https://cloud1.arc.nasa.gov/arctas/docs/presentations/Kahn_MISR_Overview.pdf (accessed on 17 May 2018).

9.   Istomina, L.G.; von Hoyningen-Huene, W.; Kokhanovsky, A.A.; Burrows, J.P. Retrieval of aerosol optical thickness in arctic region using dual-view AATSR observations. In Proceedings of the ESA Atmospheric Science Conference, Barcelona, Spain, 7–11 September 2009; pp. 1–21.

10.   Mei, L.; Xue, Y.; Kokhanovsky, A.A.; von Hoyningen-Huene, W.; Istomina, L.; de Leeuw, G.; Burrows, J.P.; Guang, J.; Jing, Y. Aerosol optical depth retrieval over snow using AATSR data. *Int. J. Remote Sens.* **2013**, *34*, 5030–5041. [CrossRef]

11.   Mei, L.; Xue, Y.; de Leeuw, G.; von Hoyningen-Huene, W.; Kokhanovsky, A.A.; Istomina, L.; Guang, J.; Burrows, J.P. Aerosol optical depth retrieval in the Arctic region using MODIS data over snow. *Remote Sens. Environ.* **2013**, *128*, 234–245. [CrossRef]

12.   Istomina, L.G.; von Hoyningen-Huene, W.; Kokhanovsky, A.A.; Schultz, E.; Burrows, J.P. Remote sensing of aerosols over snow using infrared AATSR observations. *Atmos. Meas. Tech. Discuss.* **2011**, *4*, 33–71. [CrossRef]

13.   Kokhanovsky, A.A.; Deuzé, J.L.; Diner, D.J.; Dubovik, O.; Ducos, F.; Emde, C.; Garay, M.J.; Grainger, R.G.; Heckel, A.; Herman, M.; et al. The inter-comparison of major satellite aerosol retrieval algorithms using simulated intensity and polarization characteristics of reflected light. *Atmos. Meas. Tech.* **2010**, *3*, 909–932. [CrossRef]

14.   Mei, L.; Istomina, L.; Hoyningen-Huene, W.V.; Xue, Y.; Kokhanovsky, A.A. Aerosol optical depth retrieval over Arctic region using AATSR data. In Proceedings of the 2012 IEEE International Geoscience and Remote Sensing Symposium, Munich, Germany, 22–27 July 2012; pp. 2556–2559.

15.   Holben, B.N.; Eck, T.F.; Slutsker, I.; Tanré, D.; Buis, J.P.; Setzer, A.; Vermote, E.; Reagan, J.A.; Kaufman, Y.J.; Nakajima, T.; et al. AERONET—A Federated Instrument Network and Data Archive for Aerosol Characterization. *Remote Sens. Environ.* **1998**, *66*, 1–16. [CrossRef]

16.   Holben, B.N.; Tanré, D.; Smirnov, A.; Eck, T.F.; Slutsker, I.; Abuhassan, N.; Newcomb, W.W.; Schafer, J.S.; Chatenet, B.; Lavenu, F.; et al. An emerging ground-based aerosol climatology: Aerosol optical depth from AERONET. *J. Geophys. Res. Atmos.* **2001**, *106*, 12067–12097. [CrossRef]

17.   Ångström, A. On the Atmospheric Transmission of Sun Radiation and on Dust in the Air. *Geografiska Annaler* **2017**, *11*, 156–166. [CrossRef]

18.   Flowerdew, R.J.; Haigh, J.D. An approximation to improve accuracy in the derivation of surface reflectances from multi-look satellite radiometers. *Geophys. Res. Lett.* **1995**, *22*, 1693–1696. [CrossRef]

19.   Vermote, E.F.; El Saleous, N.; Justice, C.O.; Kaufman, Y.J.; Privette, J.L.; Remer, L.; Roger, J.C.; Tanré, D. Atmospheric correction of visible to middle-infrared EOS-MODIS data over land surfaces: Background, operational algorithm and validation. *J. Geophys. Res. Atmos.* **1997**, *102*, 17131–17141. [CrossRef]

20.   Aoki, T.; Aoki, T.; Fukabori, M.; Hachikubo, A.; Tachibana, Y.; Nishio, F. Effects of snow physical parameters on spectral albedo and bidirectional reflectance of snow surface. *J. Geophys. Res. Atmos.* **2000**, *105*, 10219–10236. [CrossRef]

21.   Kokhanovsky, A.A.; Aoki, T.; Hachikubo, A.; Hori, M.; Zege, E.P. Reflective properties of natural snow: Approximate asymptotic theory versus in situ measurements. *IEEE Trans. Geosci. Remote Sens.* **2005**, *43*, 1529–1535. [CrossRef]

22.   Dumont, M.; Brissaud, O.; Picard, G.; Schmitt, B.; Gallet, J.C.; Arnaud, Y. High-accuracy measurements of snow Bidirectional Reflectance Distribution Function at visible and NIR wavelengths—Comparison with modelling results. *Atmos. Chem. Phys.* **2010**, *10*, 2507–2520. [CrossRef]

23.   Salomonson, V.V.; Appel, I. Estimating fractional snow cover from MODIS using the normalized difference snow index. *Remote Sens. Environ.* **2004**, *89*, 351–360. [CrossRef]

24.   Stohl, A.; Berg, T.; Burkhart, J.F.; Fjǽraa, A.M.; Forster, C.; Herber, A.; Hov, Ø.; Lunder, C.; McMillan, W.W.; Oltmans, S.; et al. Arctic smoke—Record high air pollution levels in the European Arctic due to agricultural fires in Eastern Europe in spring 2006. *Atmos. Chem. Phys.* **2007**, *7*, 511–534. [CrossRef]

25.   Leck, C.; Bigg, E.K. Source and evolution of the marine aerosol-A new perspective. *Geophys. Res. Lett.* **2005**, *32*, L19803. [CrossRef]

26.   Hess, M.; Koepke, P.; Schult, I. Optical Properties of Aerosols and Clouds: The Software Package OPAC. *Bull. Am. Meteorol. Soc.* **1998**, *79*, 831–844. [CrossRef]

27. Istomina, L.G.; von Hoyningen-Huene, W.; Kokhanovsky, A.A.; Burrows, J.P. The detection of cloud-free snow-covered areas using AATSR measurements. *Atmos. Meas. Tech.* **2010**, *3*, 1005–1017. [CrossRef]

28. Sogacheva, L.; Kolmonen, P.; Virtanen, T.H.; Rodriguez, E.; Saponaro, G.; de Leeuw, G. Post-processing to remove residual clouds from aerosol optical depth retrieved using the Advanced Along Track Scanning Radiometer. *Atmos. Meas. Tech.* **2017**, *10*, 491–505. [CrossRef]

29. Lyapustin, A.; Tedesco, M.; Wang, Y.; Aoki, T.; Hori, M.; Kokhanovsky, A. Retrieval of snow grain size over Greenland from MODIS. *Remote Sens. Environ.* **2009**, *113*, 1976–1987. [CrossRef]

30. Goyens, C.; Marty, S.; Leymarie, E.; Antoine, D.; Babin, M.; Bélanger, S. High angular and spectral directional reflectance dataset of snow and sea-ice. *SEANOE* **2015**. [CrossRef]